Supplementary Methods

Cell Culture and Drug Treatment

HeLa and PtK2 cells were cultured as described previously (DeLuca et al., 2005; Howell et al., 2000). For nocodazole experiments, cells were incubated in DMEM (Gibco, Carlsbad, CA) containing 20μM nocodazole for 20 min before fixation. For taxol experiments, cells were incubated in DMEM (Gibco) containing 10μM taxol for 1 h before fixation. Reductions in K-K stretch and Delta measurements to their 1 hour values due to taxol were seen in as little as 5 minutes (data not shown).

Spc24 and Spc25 Antibody Epitope Mapping

Peptide arrays (containing peptides of 15 amino acids in length with a 7 amino acid overlap) covering the entire human Spc24 and Spc25 sequences were generated (New England Peptide, Gardner, MA). Peptides were spotted on nitrocellulose and subjected to an immunoblot using polyclonal antibodies raised to Spc24 and Spc25 (McCleland et al., 2004).

Antibodies

Primary antibodies were diluted as follows in 5% boiled donkey serum: Hec1 9G3 monoclonal 1:500 (raised in mouse) (Abcam, Cambridge, MA); anti-Spc24 and -Spc25 (raised in rabbit) at 1:500 (Dr. P.T. Stukenberg, University of Virginia, McCleland et al, 2004); anti-CENP-A, and -CENP-T (rabbit) at 1:1000 (Dr. Aaron Straight, Stanford University Medical Center); anti-Bub1 (raised in sheep) and -CENP-F (rabbit) at 1:1000

(Dr. Stephen Taylor, University of Manchester); anti-hKnl1(Blinkin) mid-molecule epitope, -hKNL3h, and -hNsl1/DC31 at 1:700, anti-hKnf1/PMF1 (all rabbit) at 1:500; anti-Mis12, -CENP-I, and -CENP-C (all rabbit) at 1:500, anti-CENP-E 6A, -CENP-E Hx1, and -CENP-F at 1:1000; anti-hKnl1(Blinkin) N-terminus (mouse) at 1:20 (Dr. Mitsuhiro Yanagida, Kyoto University); and anti-GFP (rabbit) at 1:500 (Abcam). See Supplemental Table 2 for more details. All secondary antibodies (Jackson Immunoresearch, West Grove, PA) were used at 1:200 dilution in 5% boiled donkey serum.

Immunofluorescence and Fluorescence Imaging

Immunofluorescence using 4% paraformaldehyde as fixative was carried out as described previously (Howell et al., 2000), with the exception of primary antibodies to Spc24, Spc25, CENP-T, CENP-C, CENP-I, CENP-E 6A, CENP-E HX1, and CENP-F being fixed in 2% paraformaldehyde.

In short, cells were permeabilized in 0.5% Triton X-100 in PHEM buffer, fixed for 20 min in paraformaldehyde, rinsed, blocked in 5% boiled donkey serum at room temperature for 30 min, and incubated overnight in primary antibody diluted in 5% BDS at 4°C. The next morning, cells were rinsed, incubated in secondary antibodies at 1:200 dilution in 5% boiled donkey serum, rinsed, counterstained with DAPI, rinsed, and mounted on coverslips in 95% glycerol/0.5% n-propyl gallate mounting media (refractive index 1.46) (Cimini et al., 2001).

Anti-CENP-A staining required immunofluorescence using methanol as fixative as follows: Cells were placed in -20°C methanol followed by blocking in AbDil (1XTBS + 2% BSA, 0.1% Triton-X100, 0.1% NaN3). Primary antibodies diluted in AbDil were incubated overnight at 4°C. Coverslips were washed four times in AbDil. Secondary antibodies were applied to the cells for 45 minutes followed by three washes in AbDil. Cells were then placed in Hoechst diluted in AbDil followed by two washes in 1X TBS + 0.1% Triton-X. Coverslips were sealed in 95% glycerol/0.5% n-propyl gallate mounting media (Cimini et al., 2001).

For all samples, digital images were acquired using a Yokogawa (Tokyo, Japan) CSU10 Spinning Disk Confocal Fluorescence microscopy system (Maddox et al., 2003), a Nikon (Melville, NY) 100X 1.4 NA DIC Apochromatic objective, and a Hamamatsu (Hamamatsu, Japan) Orca AG cooled charge coupled device (CCD) camera at a magnification of 65 nm/pixel at the detector. Metaphase cells with metaphase plates perpendicular to the coverslip surface were identified by eye, and then red and green image pairs were acquired at 200 nm intervals along the Z-axis through the cell to obtain two-color 3D image stacks.

Delta Assay

Centroid analysis: To obtain the centroids of red and green fluorescent labels at kinetochores of sister pairs , we used nonlinear curve-fitting methods (*lsqcurvefit* in MATLAB, The Mathworks, Natick, MA) that apply to our 3D image stacks least-square curve fitting with a 3D Gaussian function (Thomann et al., 2002). This was

accomplished with a customized MATLAB program with graphical user interface (GUI) that was developed to make it easy to scroll along the z-axis through the 3D image stacks and identify sister kinetochore pairs near the same plane of focus for semi-automated analysis of the 4 centroid positions (i.e. a red and green one at each sister). The fitting volume for an individual kinetochore's fluorescence was initially set by estimation, typically 7*7 pixels and 5 frames. After the first fitting, the area was adjusted based on size from the fitting results. Then the fitting was performed again under the adjusted area. The 3D Gaussian function reports independent variances for x, y and z dimensions. Rotation transformation was also introduced to the Gaussian function. The independent variances and rotation transformation made the fitting more accurate than a simple Gaussian function. Most kinetochore fluorescence had a peak intensity of 200-400 counts (equivalent to >16000 photons collected from the entire kinetochore) above a low noise background yielding high values for the peak signal to noise ratio, (SNR > ~30). That put the accuracy of an individual centroid measurement within less than 5 nm (Thomann et al., 2002, Churchman et al., 2005, Churchman and Spudich, 2008).

Primary Delta measurement with chromatic aberration correction:

In order to correct for chromatic aberrations of the microscope, which can vary between sister kinetochore pairs, the separation distance (Delta) was calculated as an average of a sister kinetochore pair as described in Fig. 1D, where Delta is calculated from the projections of the mean separation of protein labels within each kinetochore onto the inter-kinetochore axis, which was usually determined by a line through the Hec1 9G3 centroids.

Tilt correction: Fluorescent images of kinetochores were frequently elliptical in cross-section because the face of the kinetochore was sufficiently wider than the kinetochore depth along the inner-outer axis. They often appeared tilted to the inter-kinetochore axis (Fig. 1B; Supp. Fig. 3A).

The 3D Gaussian function reported the orientations of the major and minor axes of symmetry for each kinetochore fluorescent label. These orientations were used to determine the tilt of the face of the kinetochore, theta (Θ), relative to the inter-kinetochore axis. We found for each kinetochore that the tilt angle for the red fluorescence was always nearly equal to the green fluorescence (Supp. Fig. 3B-C), indicating that all the protein linkages inbetween the red and green labels were oriented in the same way.

The mean value of Θ for a sister kinetochore pair was calculated by averaging the four tilt angles, two green tilt angles and two red tilt angles. Each tilt angle was measured by the angle between the perpendicular to the K-K axis and the long axis of the kinetochore fluorescence. The orientation of the long axis was obtained from the Gaussian fitting method, which also yielded the dimensions of the kinetochore fluorescene. Some kinetochore fluorescent images appeared round. Some had a more elliptical shape. The orientation of a round image was difficult to determine from the fitting method. Therefore, the tilt angles from round images were excluded from the tilt analysis. The threshold was set at 1.1 of the ratio between the dimensions of long axis and short axis.

Tilt was a source of error in our Delta measurements only if it was produced by inclination of kMTs and their linkages to the K-K axis (Θi in Supp. Fig. 3Di, inclination tilt). On the other hand, tilt of the kinetochore face can be produced when kMTs and their linkages within the kinetochore are parallel to the sister-sister axis, but the kMTs end at different positions as shown in Supp. Fig 3Diii (sheared tilt). This tilt, nor random differences in the relative positions of kMT ends within untilted kinetochores (Supp Fig. 3Dii) do not reduce Delta measurements from their true value if the stagger is less than about 75% of the radius of the Airy Disk (~150 nm for green light). This is because the linkages are parallel to each other and parallel to the K-K axis.

To obtain a mean value of Delta for a given pair of fluorescent labels corrected for inclination tilt, we plotted Delta values from sister kinetochore pairs with non-round fluorescent images versus their mean tilt angle (Supp. Fig. 7). We used least square fitting of the plots with the function $x = A^* \cos(Flt^*\Theta)$, where A is the average Delta value corrected for inclination tilt ($\Theta = 0$), and Flt is the average fraction of tilt that is inclination tilt (Supp. Fig. 7, Supp. Table 1).

In controls, tilt of the face of the kinetochore occurred with an average $\Theta = 15^o$, with ~50% of that value due to inclination tilt. This generated only a 1% correction. In taxol treated cells, inclination-tilt was more significant and Delta corrections of as much as 15% were required in a few cases (Supp. Table 1).

Accuracy: In addition to the tests described for the Ndc80 complex in the Results (Fig. 1E), for each average Delta value corrected for tilt we obtained the 95% confidence limits about the mean using *ttest2* in MATLAB (Table 1, Supp. Fig. 11). For pairs of average Delta values separated by 3 nm or greater, the probability they were derived from the same data population was $p<.02$.

Protein co-localization within individual kinetochores of sister pairs. Our Delta calculation assumes that the separation between a pair of labels is the same for sister kinetochores. To test this assumption, we applied the single molecule high resolution co-localization (SHREC) methods developed by Churchman, Spudich, and colleagues (Churchman et al., 2005, Churchman et al., 2006, Churchman and Spudich, 2008) for protein complexes bound to coverslip surfaces. The accuracy of this measurement depends on correction of the lateral chromatic aberration by registration of the red and green images. We first did this by imaging multi-spectrum 175nm beads (TetraSpeck, Invitrogen) bound to the objective coverslip surface. Supp. Table 3 shows the average dx and dy value between the centroids for red and green fluorophores. There was little variation within the center of the field of the camera (Supp. Table 3, SD = ~3nm) where we obtained cell images and the standard deviations were very small. We next fixed HeLa cells and then labeled 9G3 antibody with Rhodamine Red-X and Alexa-488 labeled secondary antibodies that produced nearly equal fluorescent levels. This specimen gave slightly different average dx and dy values from the beads (Supp. Table 3), probably because of the differences in fluorescent spectra. We used these average dx and dy values for the red and green labels of the 9G3 primary antibody to scale the corresponding bead

values bound to the objective coverslip surface in the image registration procedure used for SHREC. As described by Churchman and colleagues, we used the lateral chromatic aberration of the bead field to develop a two-dimensional transform for correcting local chromatic aberration of our experimental images as described in Supp. Fig. 5 A-C. This transform, based on a local weighted mean, had a target registration error (TRE, Churchman et al., 2005) of 5.8 nm. Supp. Figure 5D shows a sub-sample of the vectors separating 9G3 and Spc24-C labels of individual kinetochores after this registration. The lengths of these vectors look very similar for sister kinetochores. To test this for the whole population of sister kinetochores (n=170), for each pair we took the center position between the red 9G3 labels as the origin and the line linking the 9G3 labels as the K-K, x-axis. We then plotted the position of the center between the Spc24-C labels relative to the center (origin) of the 9G3 labels along the K-K axis as diagramed in Supp. Fig 5E to test if the variance along the K-K axis was significantly different than expected from measurements of the distance between 9G3 and Spc24-C within each kinetochore. We made similar tests for 9G3 vs. CENP-A-GFP, 9G3 vs. CENP-I, and the 9G3 Rhod Red-X/Alexa 488 double label experiment as described in detail in Supp. Fig. 5 legend.

Localization of the Kinetochore Microtubule End

For measurements of kMT ends relative to Hec1, PtK2 cells stably transfected with GFP-α-tubulin (Rusan et al, 2001) were seeded on glass coverslips in six-well plates approximately 72 hrs prior to fixation. On the day of processing, coverslips were placed in a 6°C cooler for 4-6 hours to stabilize kMT fibers and depolymerize all non-kMTs.

(Rieder, 1981)

After cold-stabilization, cells were processed as above for immunofluorescence with 2% paraformaldehyde as fixative. All steps until blocking were at 6°C to prevent regrowth of microtubules. Coverslips were blocked for 30 min at 37°C in 5% boiled donkey serum. Primary antibody incubation for Hec1 at kinetochores followed for 30 min at 37°C at a dilution of 1:600 in 5% BDS. Cells were washed 3 times in PHEM + 0.5% Triton-X 100 for 5 min each. For secondary antibody labeling, cells were incubated for 30 min at 37°C at a dilution of 1:200 in 5% BDS. Cells were washed 3 times in PHEM + 0.5% Triton-X 100 for 5 min each, counterstained with DAPI to visualize chromatin for 2 min, and washed three more times for 5 min each.

Cells could not be mounted and sealed on slides because traditional mounting techniques alters the GFP signal. Instead, cells were imaged in modified Rose chambers minus the top coverslip. The chamber was filled with PHEM buffer and the top was sealed with a 25 mm circular glass coverslip. Cells were imaged as above.

Data Analysis of kMT Fiber Linescans

For analysis, image stacks were introduced into a custom MATLAB algorithm. Linescans were taken down the axis of microtubule fibers through the estimated center of the Hec1 fluorescence. The centroid of the Hec1 fluorescence was then determined by a Gaussian fitting method. For a bundle of kMTs with ends all occurring at the same

position along the central axis of the bundle, ends are located at the point along the axial intensity profile where the fluorescence is 50% of the value above background along the axis. Axial spread in fluorescence intensity at ends is produced by diffraction within the objective that produces Airy Disk images of point sources of light. Ideally the end intensity profile will be a sigmoid of width equivalent to the diameter of the Airy Disk, which is ~420 nm in our system for green GFP fluorescence. Tilted fibers or fibers having variable ending positions produce further spreading of the fluorescence drop at the end of the kMT bundle, so they were excluded.

Since fluorescence intensity varied from cell to cell and coverslip to coverslip, the fluorescence intensity variations of the GFP-tubulin fibers over the length of the linescans were normalized on a scale from 0 to 1 so that they could be fairly compared to one another. Normalized fluorescent intensities for each kMT fiber sampled were plotted together on the Y-axis versus the position of the Hec1 centroid on the X-axis. The resulting sigmoid was fit using the equation $y = (1-\mathrm{erf}((x-a)/b))/2$, with "erf" being the error function. Coefficient "a" when $y = 0.5$ is treated as the mean distance in nm of the end of kMT fibers from the Hec1 centroid.

Supplementary Legends

Supplementary Table 1. Summary of Delta Measurements.

Results before tilt correction (Delta_uc and its SD) and after (Delta), as well as the tilt factor (Flt), 95% confidence intervals, and changes by tilt correction (|Delta| - |Delta_uc|) are listed.

Supplementary Table 2. Antibody and Reagent Detail.

Sources of antibodies as well as regions labeled within proteins are shown and cited where applicable (see Supplementary References).

Supplementary Table 3. Average Chromatic Aberration Measurements.

Chromatic aberration was measured for beads and for Red-Green labeled Hec1 9G3 kinetochores. See Supp. Methods for details.

Supplementary Figure 1. Epitope Mapping of Spc24 Antibody.

A peptide array comprising the sequences of human Spc24 and Spc25 were adsorbed onto nitrocellulose and immunoprobed with Spc24 antibody. As a control, HeLa extract was adsorbed onto the nitrocellulose at region G12. The antibody recognized 3 spots in the C-terminal region of Spc24 sequence as well as the positive control. At right is the hSpc24 sequence with recognized peptide sequence in red. Two experiments are shown.

Supplementary Figure 2. Epitope Mapping of Spc25 Antibody.

A peptide array comprising the sequences of human Spc24 and Spc25 were adsorbed onto nitrocellulose and immunoprobed with Spc25 antibody. As a control, HeLa extract was adsorbed onto the nitrocellulose at region G12. The antibody recognized 1 spot at the N-terminus of Spc24 sequence and 4 spots near the C-terminus of Spc25. At right are the hSpc24 and hSpc25 sequences with recognized peptide sequences in red, blue, and pink. Two experiments are shown. By immunofluorescence, the Spc25 antibody does not appear to recognize the N-terminal epitope of Spc24 since Delta measurements for anti-Spc24, which recognizes only C-terminal epitopes (Supp Fig. 1) vs. Hec1 9G3 were identical to measurements for anti-Spc25.

Supplementary Figure 3. Analysis of Tilt for Red vs. Green Labels.

(A) Tilt detection from 3-D Gaussian fitting, shown by blue lines. (B) Tilt angles of 9G3 and Spc24-C of control cells. (C) Tilt angles of red and green labels from all the control cells. (D) Potential tilting of protein linkages: (i) Inclination tilt, Θi; (ii) Randomly staggered ends with Θi = 0; (iii) Sheared staggered ends with Θi = 0.

Supplementary Figure 4. Signal Intensity.

(A) Images of 9G3 and Spc24-C. (B) Line scan of 9G3 signal along K-K axis. (C) Line scan of Spc24-C along K-K axis. The images and line scan show a peak signal of 250-350 counts above background noise (SD = 8). This yields a high signal-to-noise ratio of 31-44.

Supplementary Figure 5. Co-localization of Fluorescent Labels within Individual Kinetochores of Sister Pairs by SHREC to Test if Distances are the Same and Equal to Values Measured in the Delta Assays.

(A) Red to green vectors for bead array bound to the objective coverslip surface before registration. The vector length was drawn 20 times its actual length for better visualization. (B) Vectors after registration (80 times actual vector length). (C) Polar plot for both unregistered (blue) and registered (red) vectors. (D) Vectors of 9G3 to Spc24 for individual kinetochores of sister pairs in a sample of the population analyzed after correction for lateral chromatic aberration as described in Supp. Methods (8 times actual vector length). (E) A diagram showing the vector (Vm) between the middle point of the centroids of 9G3 labels on sister kinetochores and the middle point of the centroids of Spc24-C labels for the same pair; the K-K axis extends between the 9G3 labels for each sister pair. (F) Vm vector plot for 9G3 and Spc24-C. (G) Vm vector plot for 9G3 and CENP-A-GFP. (H) Comparison among different measurements. The distance between 9G3 and the three other protein labels was measured for individual kinetochores by the SHREC method (Churchman and Spudich, 2005, 2008) with Maximum Likelihood (Churchman et al., 2006) correction. The results were very similar to the Delta measurements obtained from sister kinetochore pairs. However, errors introduced by the registration to correct for lateral chromatic aberration (TRE = 5.8, see Supp. Methods) made the SD of the SHREC distance higher than the SD of Delta for all 3 protein measurements. The standard deviation (SD) of the Vm vector projection on the K-K axis (Vm_kk) was calculated and compared with the standard deviation of Delta. Similar tests were also conducted for CENP-A-GFP and CENP-I. Almost identical results for Spc24

and CENP-I (rigid by Delta analysis) shows no clear difference within a sister pair showing they exhibit the same values. The lower SD for CENP-A-GFP (compliant by Delta analysis) is particularly significant. This shows that the sister kinetochores exhibit the same compliance since the middle point of CENP-A-GFP tends to stay in the same place over a wide range of stretch and the SD for center movement is smaller than the SD of Delta.

Supplementary Figure 6. Maps of Key Epitopes on Large Proteins.

Graphical representations of antigens and key structural features relevant to our measurements for (A) hKnl1/Blinkin; (B) CENP-E; (C) CENP-F; and (D) Bub1. For further antibody information, see Supplementary Methods and Supplementary Table 2.

Supplementary Figure 7. Tilt Plots for All Measurements.

Delta before tilt correction (nm, Y-axis in all plots) was plotted as a function of tilt angle theta (degrees, X-axis in all plots) for a subset of the data where tilt angle could be identified. Least-square fitting lines for each protein linkage to function $x = A*cos(Flt*theta)$ are plotted onto figures, with A corresponding to intercept at theta = 0. A equals the average value of Delta corrected for inclination tilt. (A) Control measurements. (B) Measurements for cells treated with 10 μM taxol for 1 hr prior to fixation.

Supplementary Figure 8. Delta Plots for All Measurements.

Delta before tilt correction (nm, Y-axis in all plots) was plotted as a function of K-K measured between Hec1 9G3 centroids of sister kinetochores (μm, X-axis in all plots). (A) Control measurements. (B) Measurements for cells treated with 10 μM taxol for 1 hr prior to fixation.

Supplementary Figure 9. KMT Fiber Orientation.

Histogram showing uniform distribution of kMT fiber orientation angle relative to the horizontal image axis for the data set. Even sampling of fibers from all orientations ensured additional measurement errors due to chromatic aberrations in the optics were minimal.

Supplementary Figure 10. Centromeric Chromatin Compliance and Assembly of Multiple Attachment Site Kinetochores.

A. Depth and Compliance of CENP-A and CENP-C within the peripheral centromeric chromatin in comparison to the stiff kinetochore during chromosome oscillations. Using CENP-I as a marker for the peripheral surface of the centromeric chromatin, at minimal centromere stretch, the separation between the centroids of CENP-I and CENP-C was ~11 nm and the centriods of CENP-I and CENP-A ~30 nm. Assuming uniform distribution, these numbers indicate total depths of 22 nm for CENP-C and ~60 nm for CENP-A. At maximal centromere stretch, these depths increase to 46 nm and 128 nm respectively. The region of the centromere containing CENP-A appears to be about twice the stiffness of the bulk of the centromeric chromatin.

B. Speculative Model for how the Kinetochore is Built from Multiple kMT Attachment Sites. Kinetochores with multiple attachment sites are constructed from a two-dimensional parallel array of chromatin fibers that extend along the K-K axis at metaphase, each with kinetochore protein complexes assembled at their peripheral tips. To account for the anisotropic properties of the kinetochore and peripheral centromere (strong along the inner-outer axis and weak laterally), we suggest that a kinetochore microtubule attachment site is primarily linked to one or a few chromatin fibers at their peripheral tips where the path of the DNA changes from an outside to an inside direction (Yeh et al., 2008). Mechanical anisotropy at the centromere periphery results from weak lateral linkages (yellow rectangles) between neighboring chromatin fibers and potentially in between their kMT attachment sites. There are several points of similarity of the proposed side-by-side attachment sites to published high resolution tomographs (Dong et al., 2007). These include the low contrast gap, and a 45 nm thick outer plate mainly defined by the 45 nm axial length of the bent Ndc80 complex. The horizontal arms of the Ndc80 and Mis12 complexes could produce the horizontal filaments reported near the inner surface of the outer plate in electron micrographs (Dong et al., 2007).

Supplementary Figure 11. Statistical Analysis of Average Delta Values.
Statistical significance between any two different delta measurements was calculated by paired t-test (*ttest2* in MATLAB). The difference between the two measurements was characterized by their mean value difference. Statistical significance was represented by a number between 1 and 0 (the p-value).

	Delta_uc	SD	n	SEM	CI (%95 +/-)	A	Flt	Delta	SD	n	|Delta| - |Delta_uc|
control											
Spc24-C	44	7	176	0.5	1	45	0.79	45	6	107	1
Bub1-NM	27	8	182	0.6	1.2	26	0	26	8	123	-1
Cenp-A-GFP	105	14	172	1.1	2.2	107	0.49	107	14	116	2
Spc25	44	4	147	0.3	0.7	45	0.69	45	4	131	1
KNL3/hMis13/Dsn1-C	46	7	276	0.4	0.8	47	0.62	47	7	159	1
hNsl1/DC31/hMis14	48	5	97	0.5	1	49	0.84	49	5	80	1
hNnf1/PMF1	56	6	141	0.5	1.1	56	0.47	56	7	64	0
Mis12	47	6	149	0.5	0.9	48	0.71	48	6	134	1
hKNL1/AF15q14/Blinkin-M	34	6	77	0.7	1.4	34	0	34	6	63	0
CENP I	61	8	115	0.8	1.5	62	0.78	62	7	69	1
CENP T	59	5	210	0.4	0.7	59	0.59	59	5	120	0
CENP C	79	10	231	0.6	1.2	79	0.52	79	10	141	0
Cenp E-MC	-5	18	122	1.6	3.2	-3	0	-3	16	64	-2
Cenp E-NM	-11	14	209	1	1.9	-13	1.51	-13	15	107	2
CLASP	-29	9	22	1.9	3.7	-29	0	-29	9	18	0
9G3 Red vs Green	0	4	117	0.4	0.8	0	0.02	0	5	91	0
Cenp F-C	-4	10	172	0.7	1.4	-4	0	-4	10	97	0
Cenp F-M	-46	11	121	1	1.9	-48	0.19	-48	10	54	2
Hec1-GFP	2	8	121	0.7	1.4	3	-0.01	3	7	44	1
taxol											
Spc24-C	45	11	167	0.8	1.7	45	0.46	45	11	46	0
Bub1-NM	17	13	64	1.6	3.2	18	0	18	14	28	1
Cenp-A-GFP	72	17	129	1.5	2.9	78	0.88	78	15	61	6
Spc25	44	17	37	2.8	5.5						
KNL3/hMis13/Dsn1-C	30	12	157	1	1.9	35	1.14	35	12	63	5
hNsl1/DC31/hMis14	42	11	93	1.1	2.2	49	1.03	49	12	35	7
hNnf1/PMF1	52	9	68	1.1	2.2	54	0.94	54	8	39	2
Mis12	38	11	111	1	2	44	1.34	44	12	66	6
hKNL1/AF15q14/Blinkin-M	24	10	93	1	2	24	0.83	24	10	40	0
CENP I	47	9	83	1	2	47	0.88	47	8	28	0
CENP T	41	11	140	0.9	1.8	43	0.76	43	11	29	2
CENP C	56	11	106	1.1	2.2	57	0.38	57	11	51	1
Cenp E-MC	-8	19	79	2.1	4.2	-12	1.89				
Cenp E-NM	-35	17	63	2.1	4.2	-33	0	-33	18	19	-2
CLASP	-40	11	11	3.4	6.6	-40	0.83	-40	12	10	0
Cenp F-C	-14	15	127	1.4	2.7	-14	0	-14	17	50	0
Cenp F-M	-60	20	98	2	3.9	-57	0	-57	18	39	-3

Supplementary Table 1

Supplementary Table 2 – Antibody/reagent detail

Protein	Antibody	Antigen	MW (kDa)	Coiled-Coil Domains	AA #	Source
CENP-A	Rabbit anti CENP-A	Full Length	17	Weak or none	140	Aaron Straight (unpublished)
CENP-A-GFP	Rabbit anti GFP	GFP	17	weak or none	140	Jan Ellenberg (Gerlich et al., 2003)
CENP-C	Rabbit anti CENP C	unknown	140	weak or none	943	Tim Yen (Liu et al., 2006)
CENP-I	Rabbit anti CENP I	N-term 249	87	weak or none	756	Tim Yen (Liu et al., 2003)
CENP-T	Rabbit anti CENP T	Full Length	34	320-360	561	Aaron Straight (unpublished)
hNnf1/PMF1	Rabbit anti hNnf1/PMF1	Full Length	23.3	weak or none	220	Arshad Desai (Kline et al., 2006)
hNsl1/DC31/hMis14	Rabbit anti hNsl1/DC31	22-281	32.2	weak or none	281	Arshad Desai (Kline et al., 2006)
Mis12	Rabbit anti hMis12	Full Length	24.1	100-150, 175-205	205	Tim Yen (Liu et al., 2006)
KNL3/hMis13/Q9H410/Dsn1-C	Rabbit anti hKNL3 (hDsn1)	181-356	40.1	weak or none	356	Arshad Desai (Kline et al., 2006)
hKNL1/AF15q14/Blinkin-M	Rabbit anti hKNL1	~1220-1440	265.3	1900-2200	2342	Arshad Desai (Cheeseman et al., 2008)
Knl1/Blinkin/AF15q14-N	Mouse anti Blinkin	N-term 22	265.3	1900-2200	2342	M. Yanagida (Kiyomitsu et al., 2007)
Bub1-NM	Sheep anti Bub1	336-489	123	275-300, 1050-1100	1085	Steve Taylor (Taylor et al., 2001)
Spc24-C	Rabbit anti Spc24	Full Length	22.4	20-130	197	Todd Stukenberg (McCleland et al., 2004)
Spc25	Rabbit anti Spc25	Full Length	26.1	50-150	224	Todd Stukenberg (McCleland et al., 2004)
Hec1	Mouse Mab9G3	200-222	73.9	240-420, 460-580,600-642	642	Abcam
GFP-Hec1	Rabbit anti-GFP	GFP	73.9	240-420, 460-580,600-642	642	Walt Gall (DeLuca et al., 2006)
CENP-F-M	Sheep anti CENP F	1363-1640	367	1-1400, 1550-1700, 1800-2900	3114	Steve Taylor (Hussein et al., 2002)
CENP-F-C	Rabbit anti CENP F	C-term 561	367	1-1400, 1550-1700, 1800-2900	3114	Tim Yen (Liao et al., 1995)
CENP-E-NM	Rabbit anti CENP E 6A	663-973	312	300-400, 500-2600	2663	Tim Yen (Zecevic et al., 1998)
CENP-E-MC	Rabbit anti CENP E Hx1	1571-1859	312	300-400, 500-2600	2663	Tim Yen (Chan et al., 1998)

	dx (SD) (nm)	dy (SD) (nm)
Beads (coverslip surface)	-28 +/- 3.2	28.4 +/- 3.4
Centroids of RedX and Alexa 488 bound by antibodies to 9G3	-31 +/- 9.6	32.9 +/- 9.7

Supplementary Table 3

Spc24 antibody

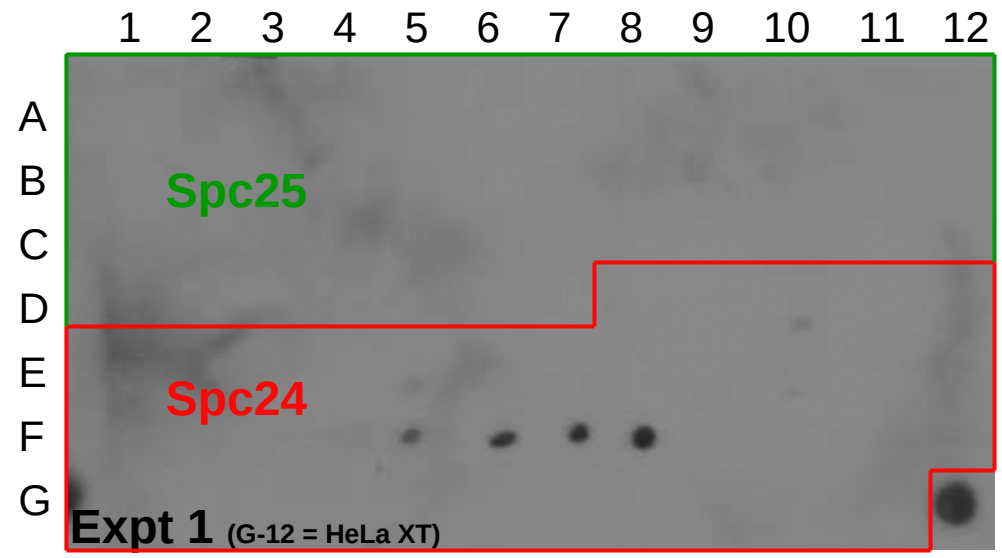

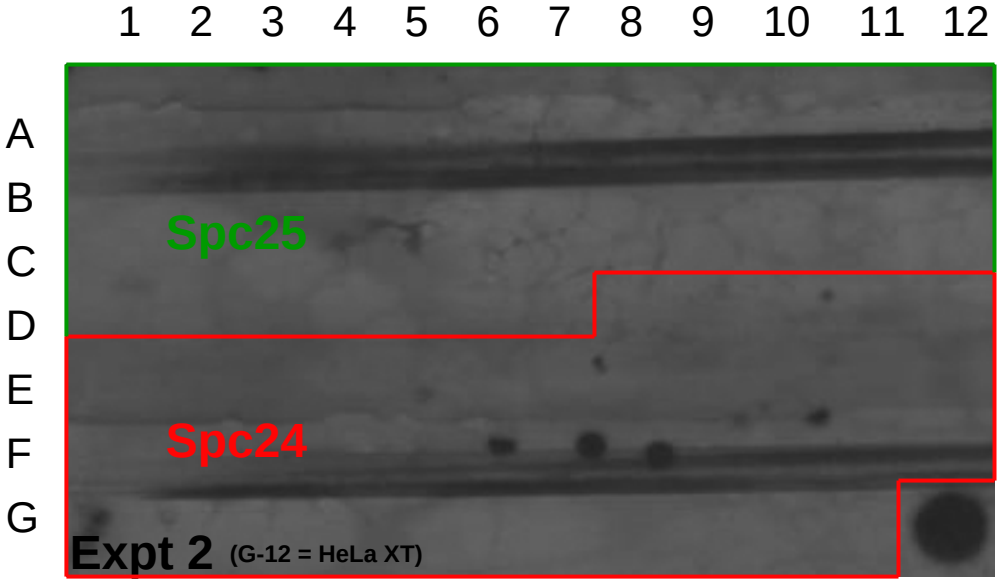

*Spc24 antibody recognizes 3 spots in series at amino acids 111-135 (red)

Spc24
1 maafrdieev sqgllsllga nraeaqqrrl lgrheqvver lletqdgaek qlreiltmek
61 evaqsllnak eqvhqggvel qqleaglqea geedtrlkas llqltrelee **lkeieadler**
121 **qekevdedtt vtips**avyva qlyhqvskie wdyecepgmv kgihhgpsva qpihldstql
181 srkfisdylw slvdtew

Supplementary Figure 1

Spc25 antibody

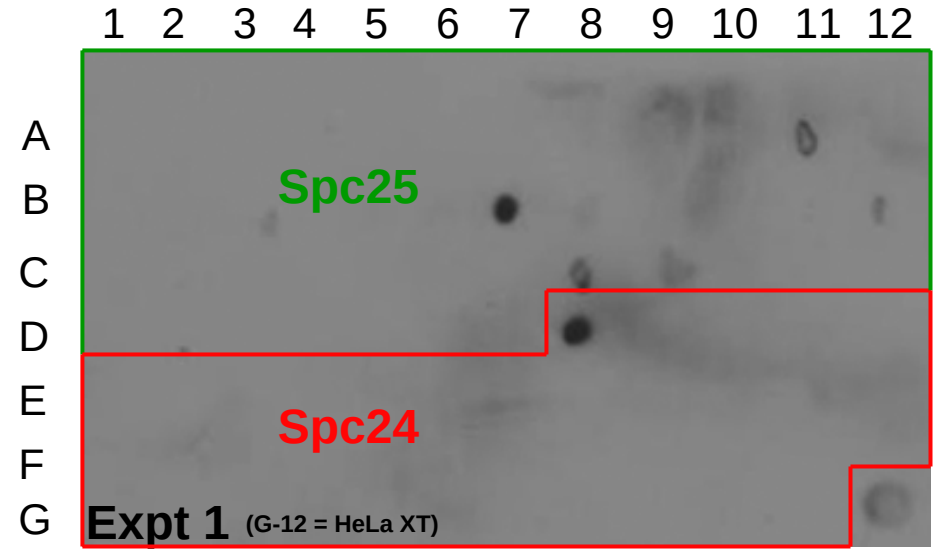

*Spc25 antibody recognizes 2 major spots on the blot: one peptide from Spc24 at amino acids 1-15 and one peptide from Spc25 at amino acids 91-105 (in blue). These two spots were of equal intensity.The antibody recognizes a fainter 2-spot series at amino acids 156-176 (pink) within Spc25. These results are consistent with the second blot, although the spots at C8, C9 (aa 156-176, pink) are more intense.

Spc24
1 maafrdieev sqgllsllga nraeaqqrrl lgrheqvver lletqdgaek qlreiltmek
61 evaqsllnak eqvhqggvel qqleaglqea geedtrlkas llqltrelee lkeieadler
121 qekevdedtt vtipsavyva qlyhqvskie wdyecepgmv kgihhgpsva qpihldstql
181 srkfisdylw slvdtew

Spc25
1 mvedelalfd ksinefwnkf kstdtscqma glrdtykdsi kafaeklsvk lkeeermvem
61 fleyqnqisr qnkliqekkd nllkliaevk gkkqelevlt aniqdlkeey srkketista
121 nkanaerlkr lqksadlykd rlgleirkiy geklqfiftn idpknpespf mfslhlnear
181 dyevsdsaph leglaefqen vrktnnfsaf lanvrkafta tvyn

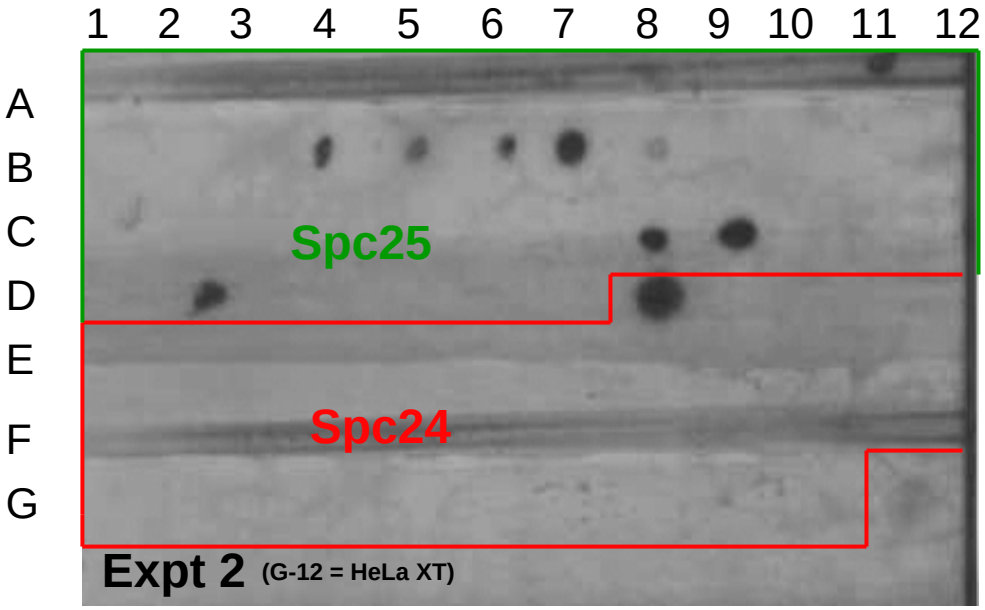

Supplementary Figure 2

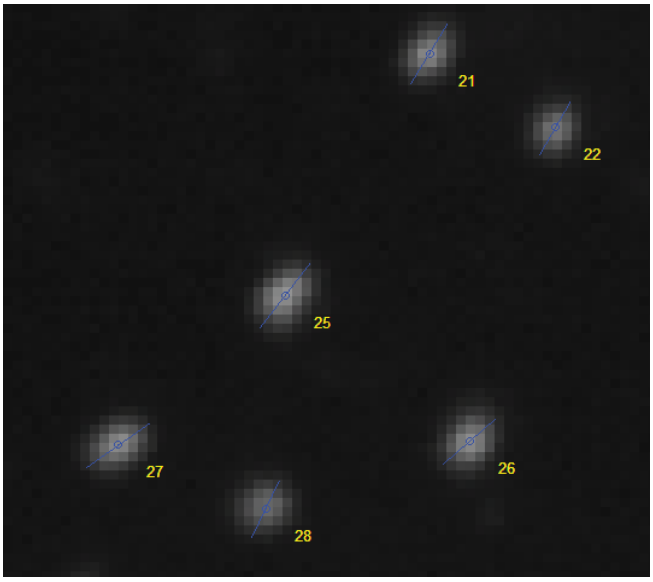

A

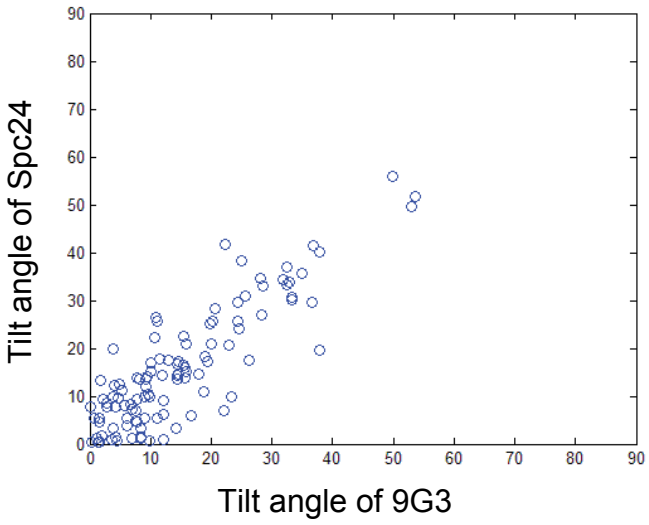

B

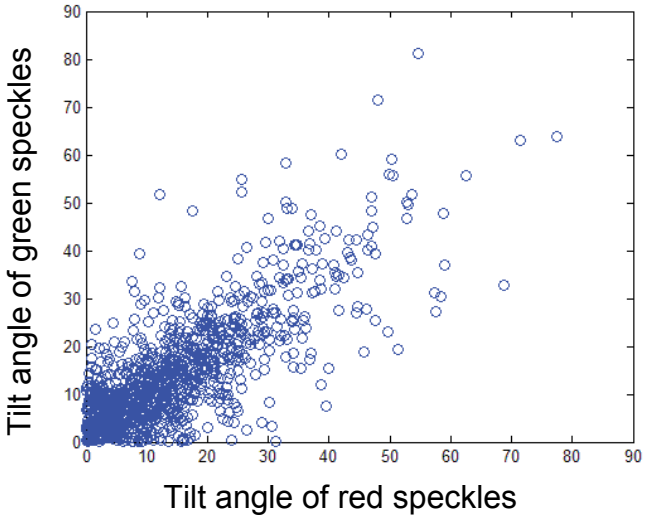

C

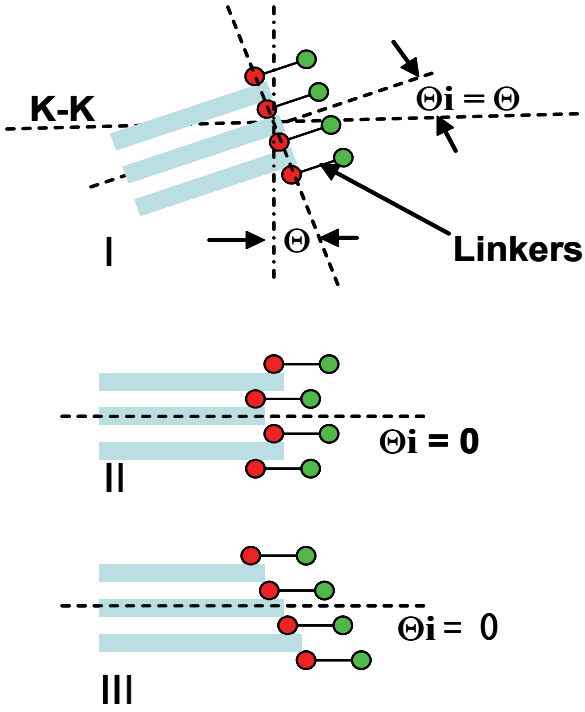

D

Supplementary Figure 3

A

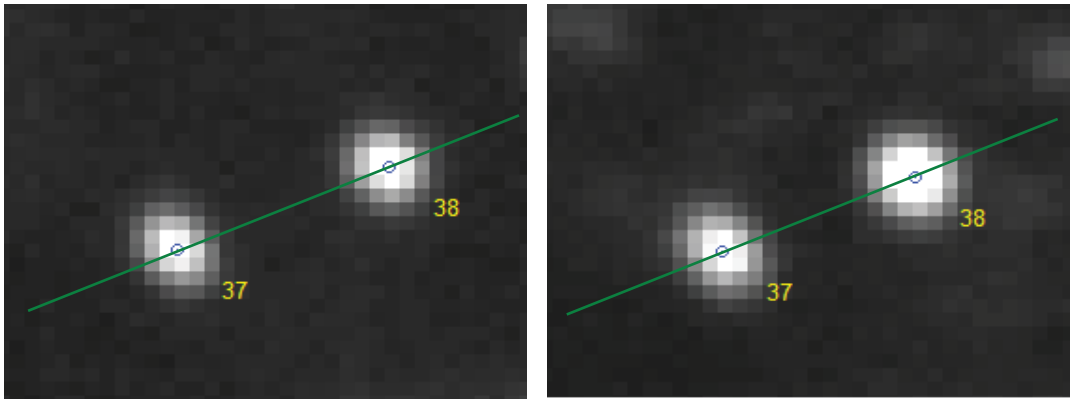

9G3 Spc24-C

B

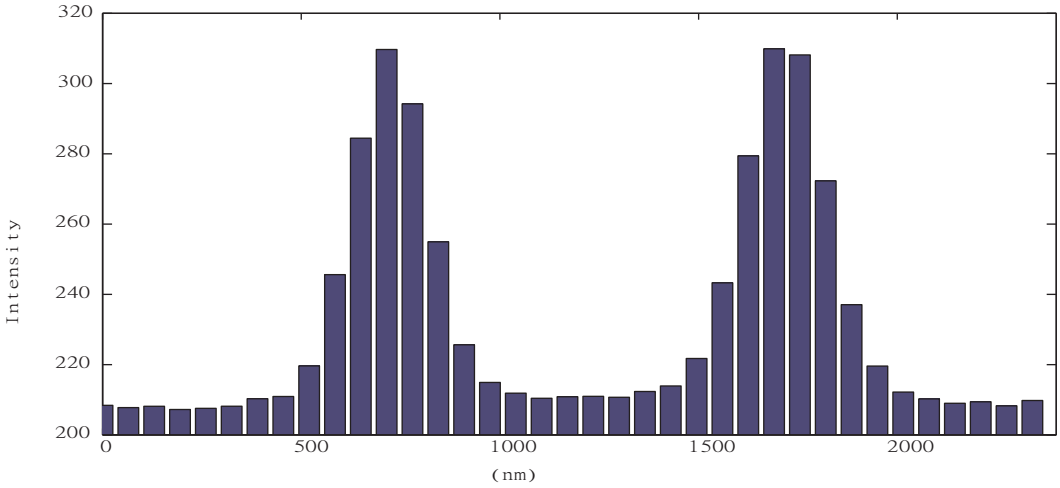

C

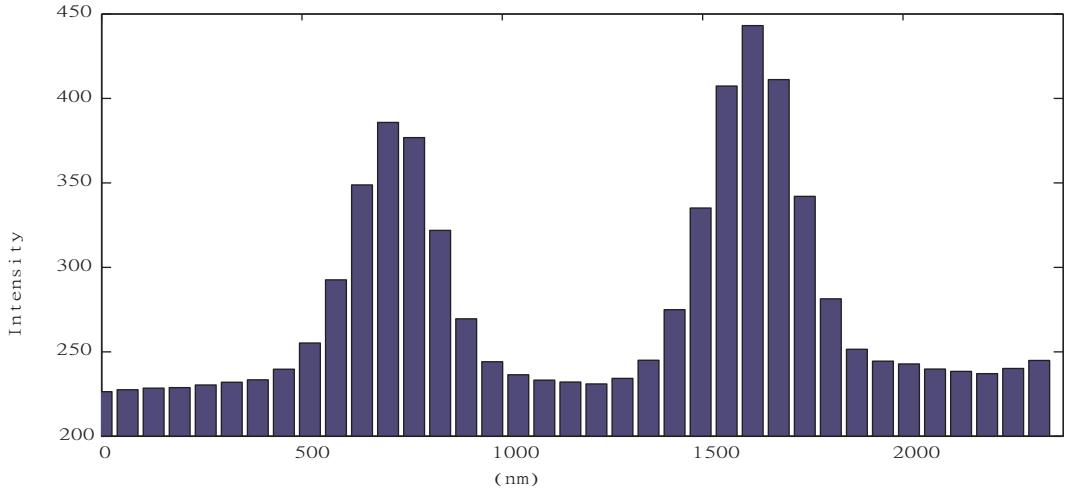

Supplementary Figure 4

A

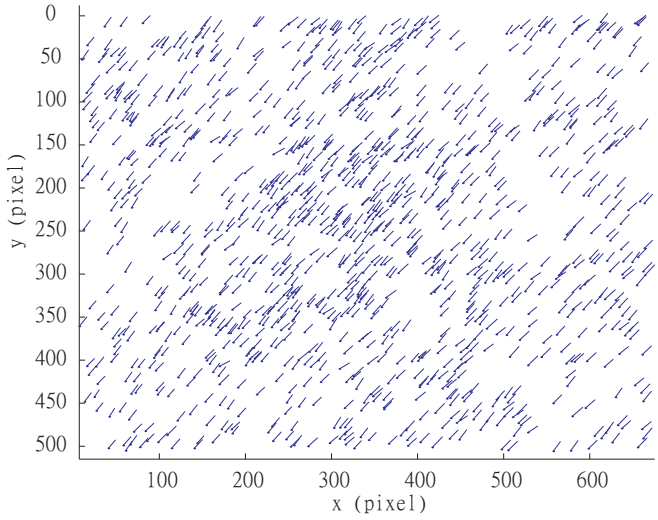

B

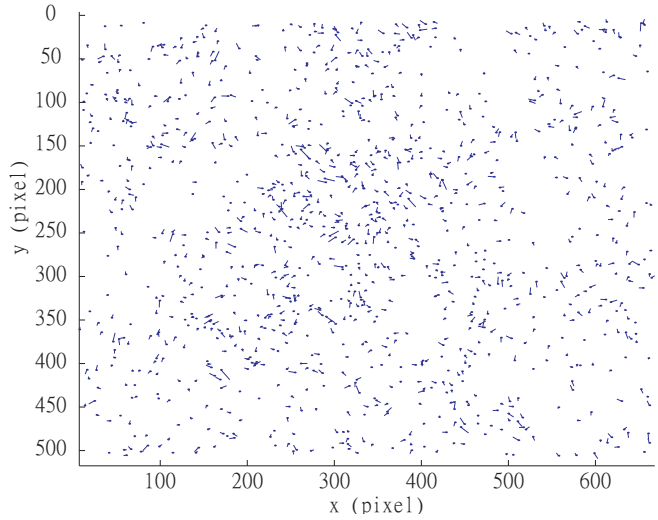

C

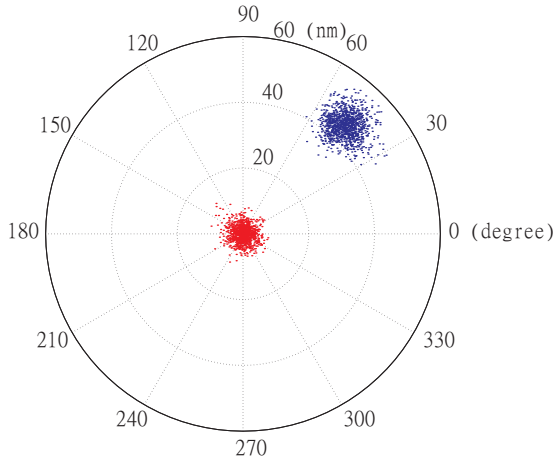

Supplementary Figure 5

D

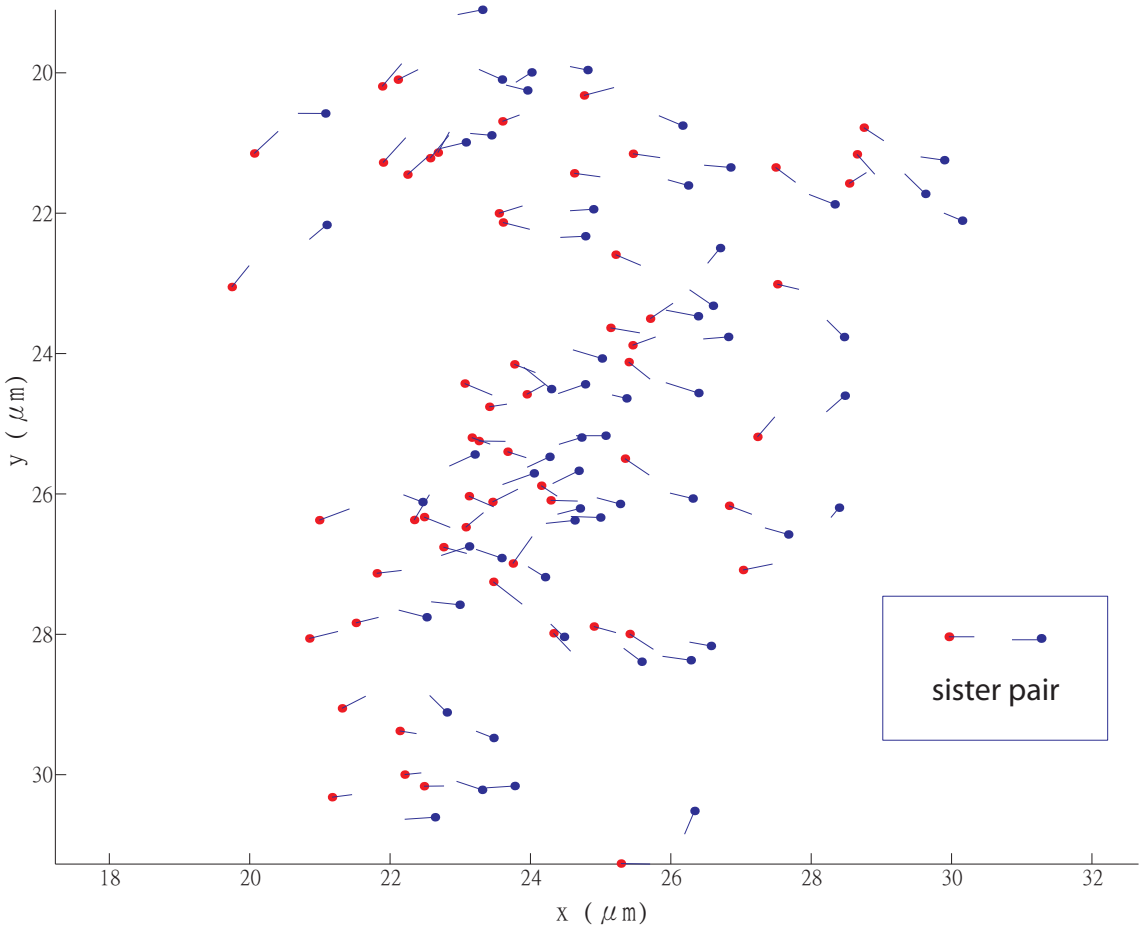

E

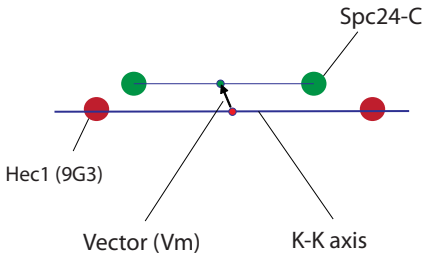

F

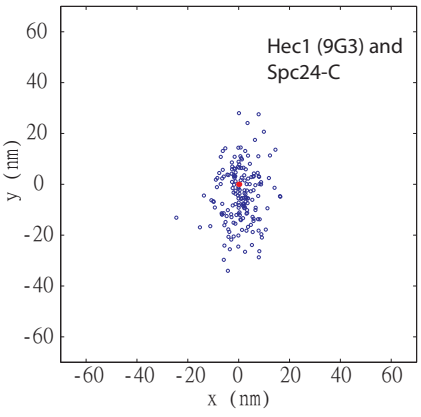

G

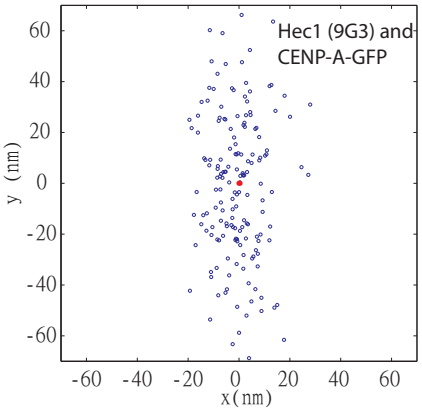

H

	Delta (nm)	SHREC (nm)	SD (Vm_kk) (nm)
(Hec1) 9G3 - Spc24-C	45 +/- 6.6	46 +/- 8.9	6.2
(Hec1) 9G3 - Cenp-A-GFP	107 +/- 14.5	108 +/- 17.7	8.9
(Hec1) 9G3 - CENP-I	62 +/- 8.2	63 +/- 12.9	9

Supplementary Figure 5

A

B

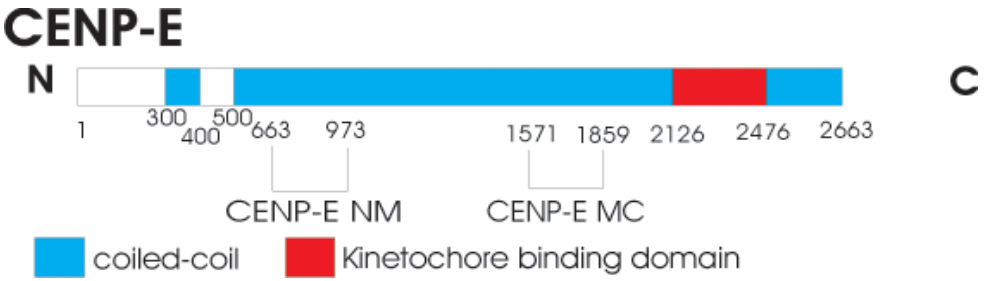

C

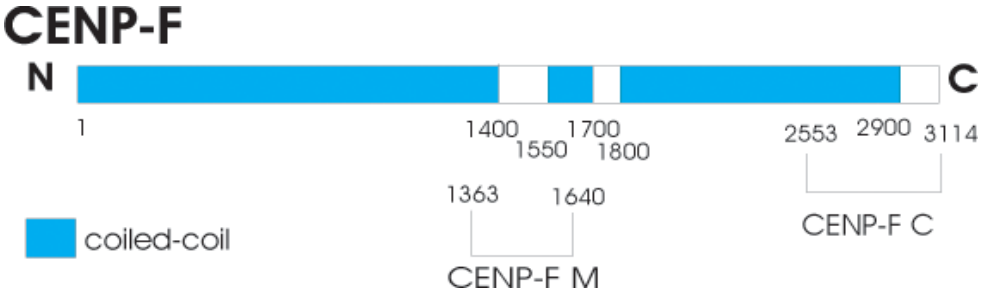

D

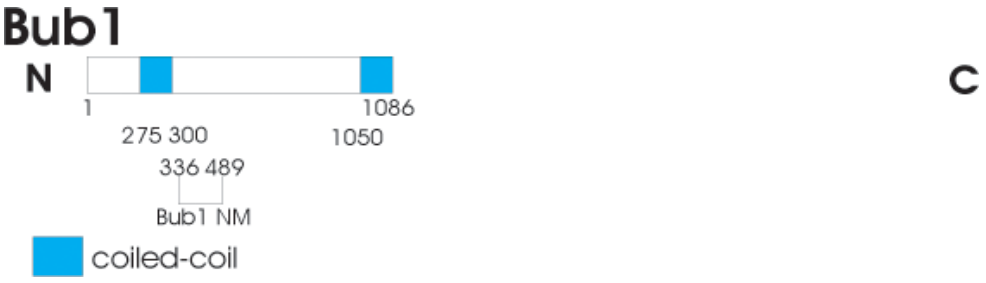

Supplementary Figure 6

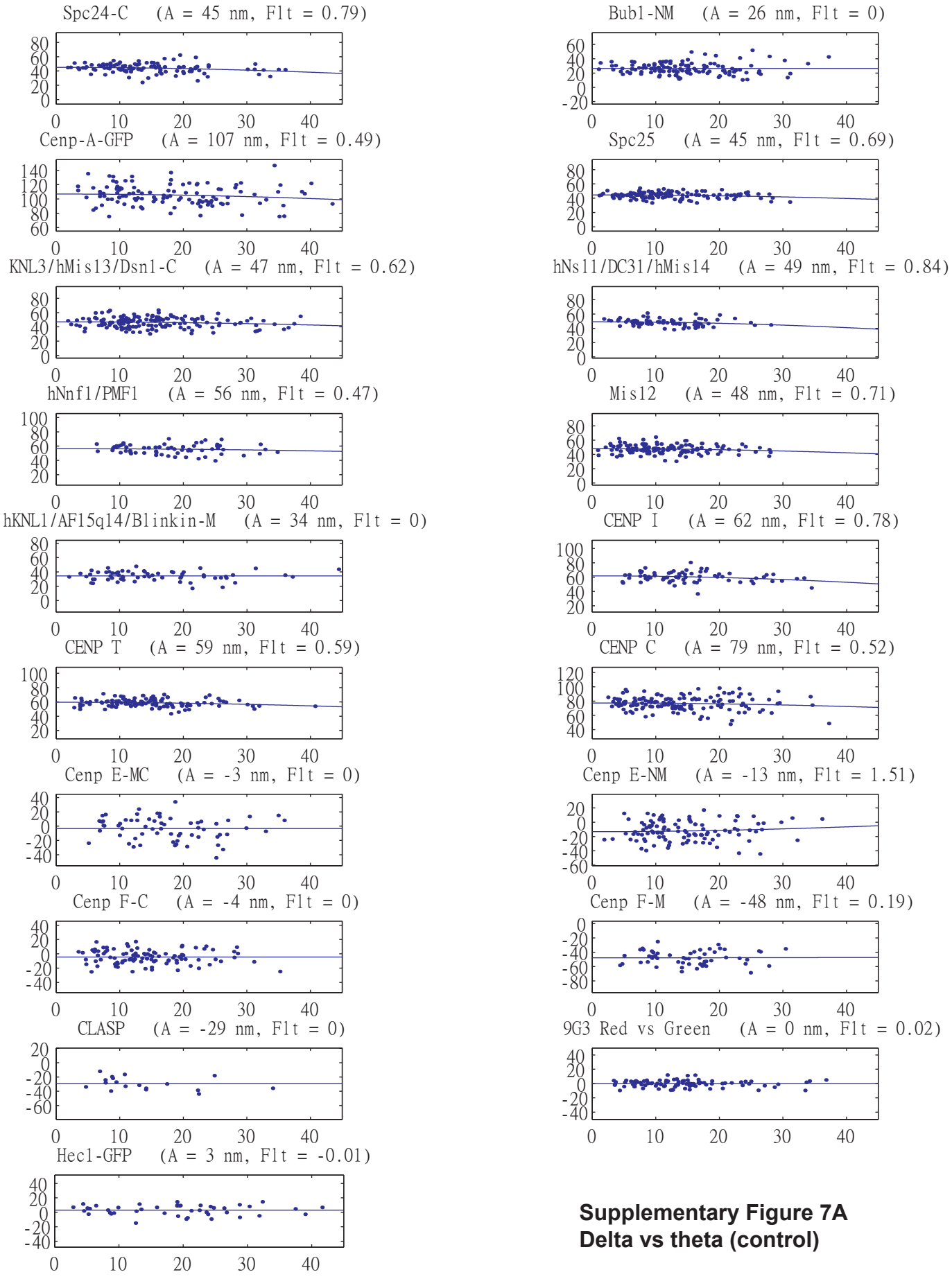

Supplementary Figure 7A
Delta vs theta (control)

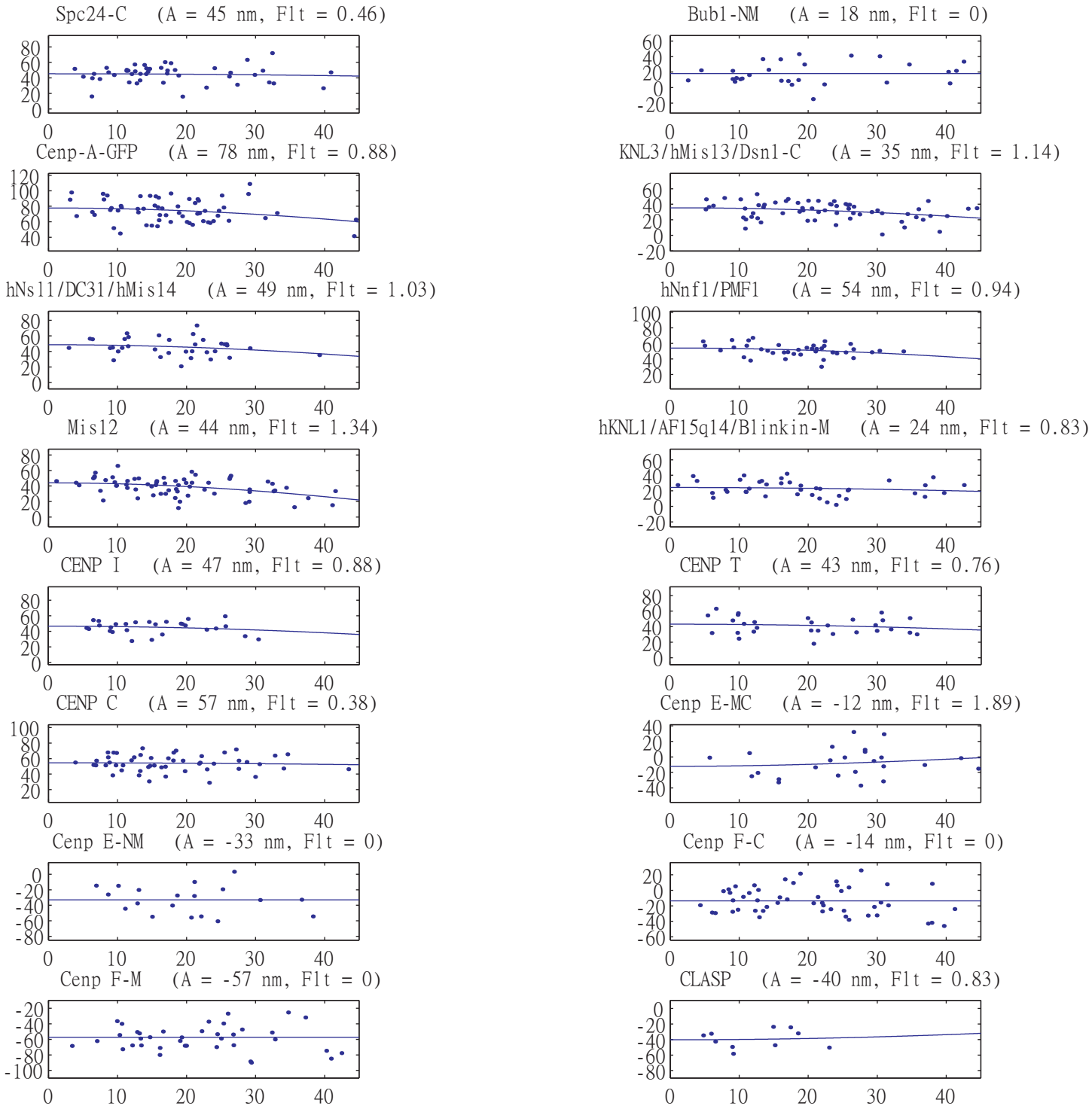

Supplementary Figure 7B
Delta vs theta (taxol)

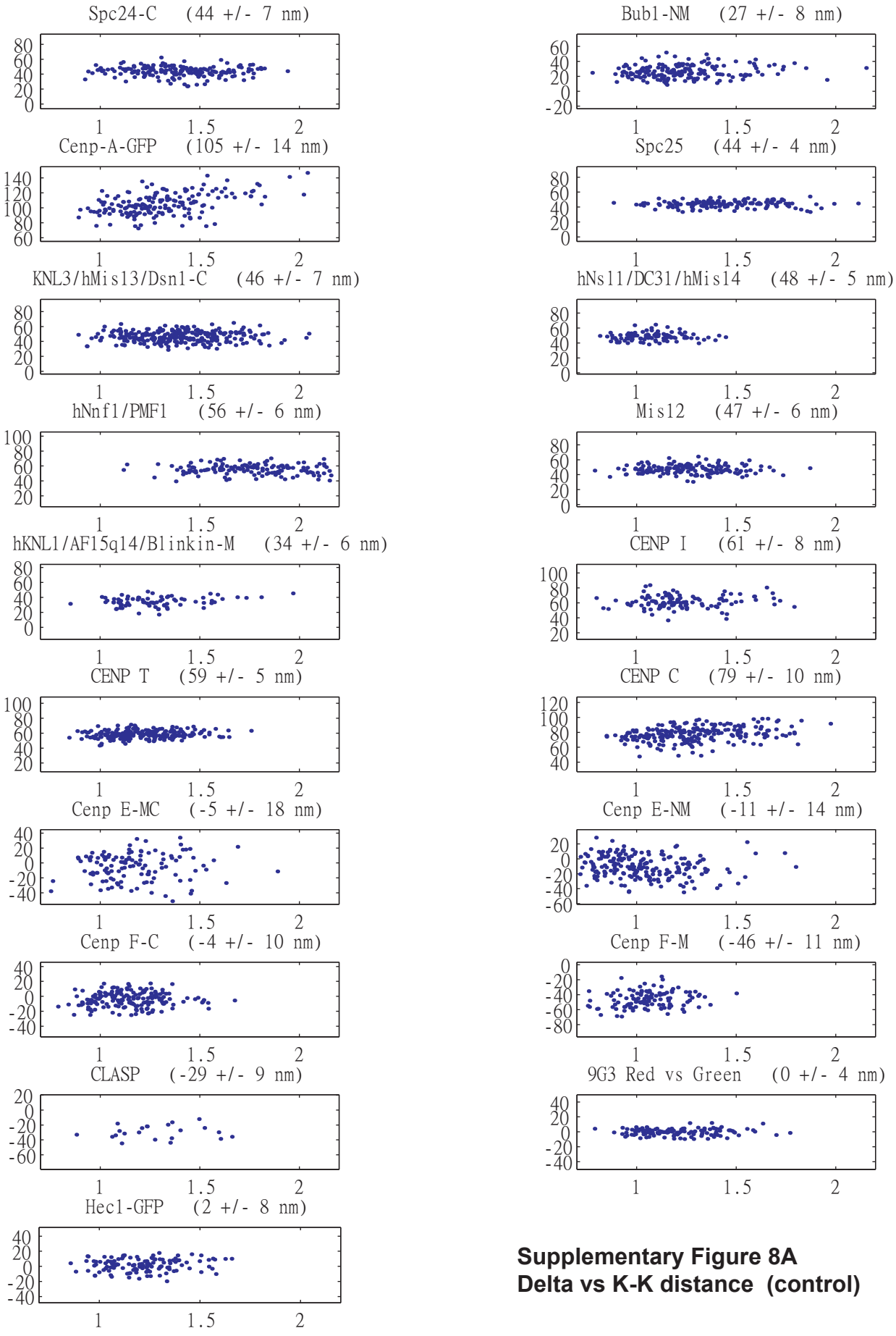

Supplementary Figure 8A
Delta vs K-K distance (control)

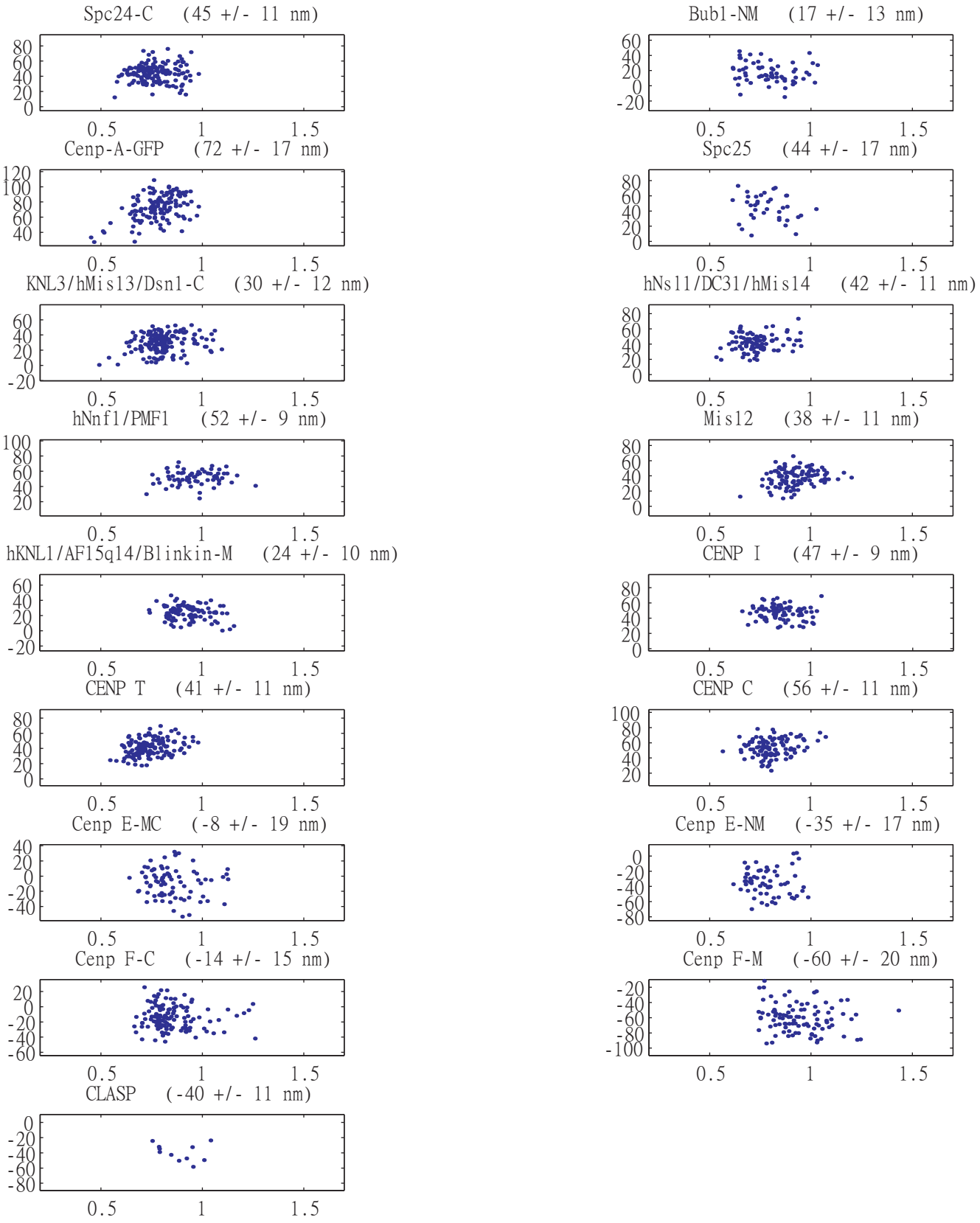

Supplementary Figure 8B
Delta vs K-K distance (taxol)

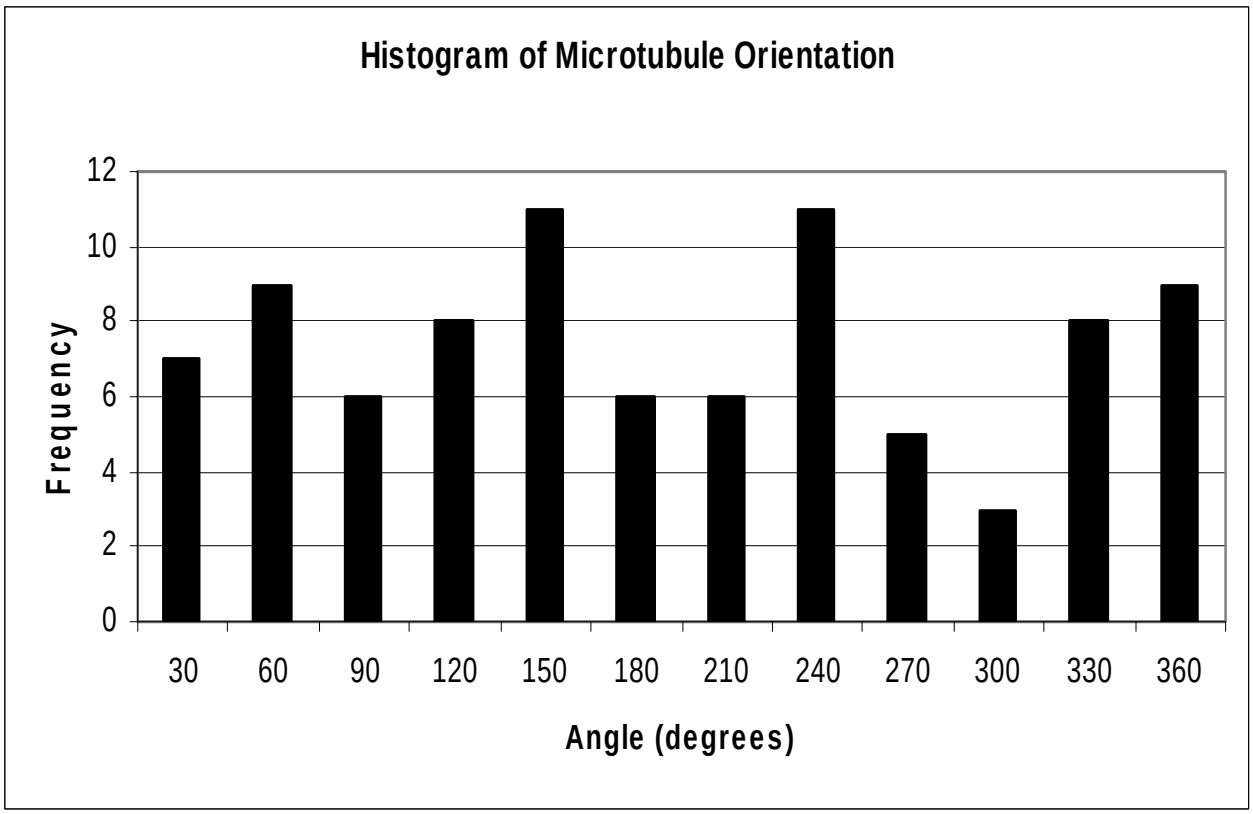

Supplementary Figure 9

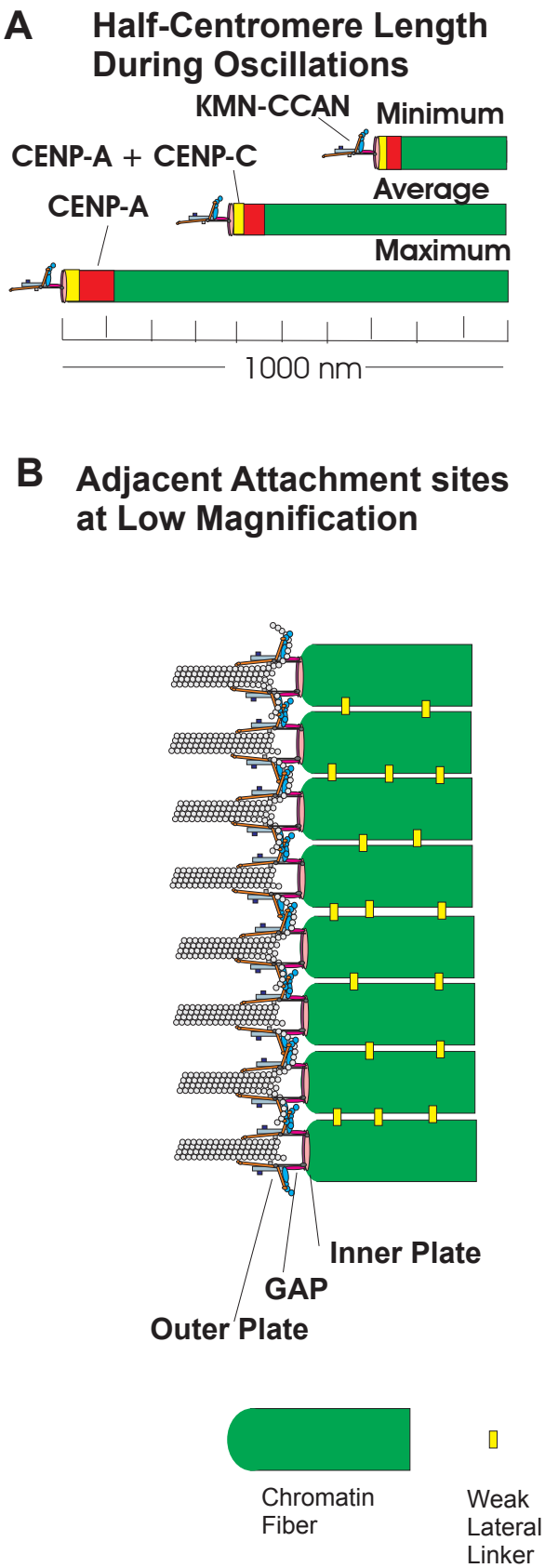

Supplementary Figure 10

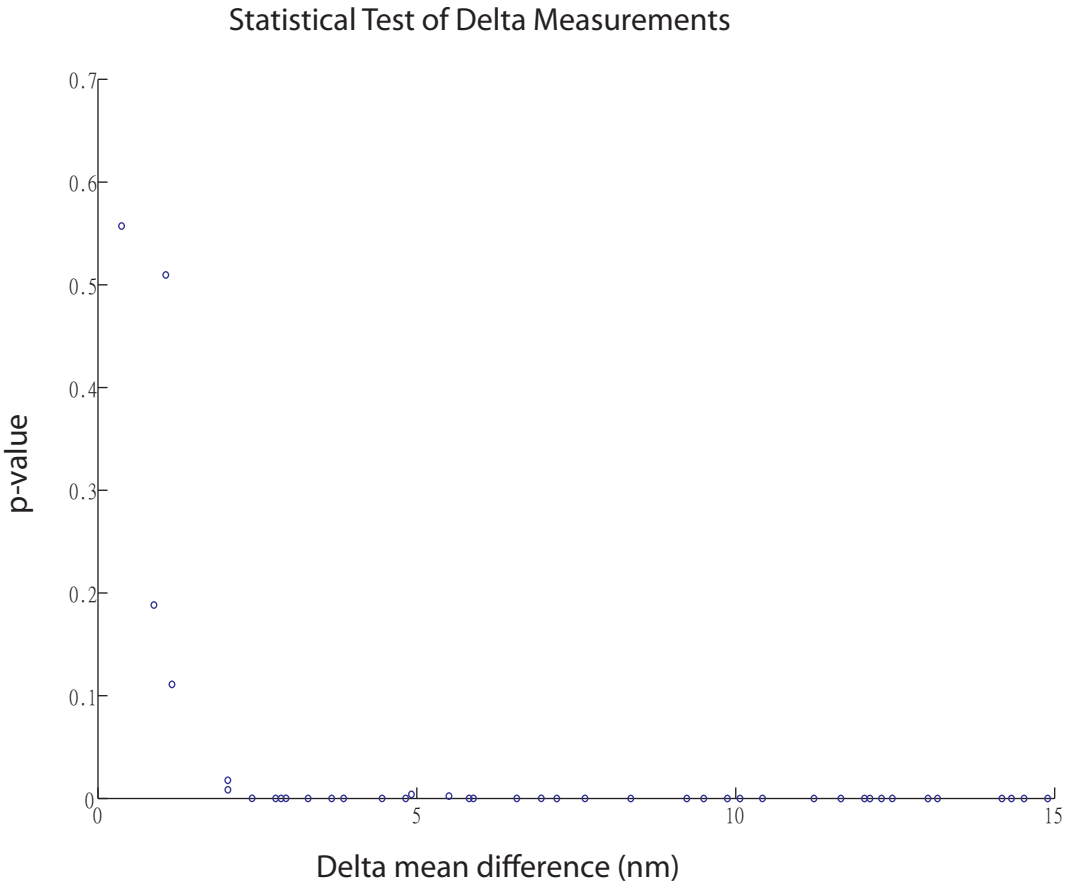

Supplementary Figure 11

Supplementary References

Chan, G.K., Schaar, B.T., and Yen, T.J. (1998). Characterization of the kinetochore binding domain of CENP-E reveals interactions with the kinetochore proteins CENP-F and hBUBR1. J Cell Biol *143*, 49-63.

Cheeseman, I.M., Hori, T., Fukagawa, T., and Desai, A. (2008). KNL1 and the CENP-H/I/K Complex Coordinately Direct Kinetochore Assembly in Vertebrates. Mol Biol Cell *19*, 587-594.

Churchman, L.S., Okten, Z., Rock, R.S., Dawson, J.F., and Spudich, J.A. (2005). Single molecule high-resolution colocalization of Cy3 and Cy5 attached to macromolecules measures intramolecular distances through time. PNAS *102*, 1419-1423.

Churchman, L.S., Flyvbjerg, H., and Spudich, J.A. (2006). A non-Gaussian distribution quantifies distances measured with fluorescence localization techniques. Biophys J *90*, 668-671.

Churchman, L.S., and Spudich, J.A. (2008). Colocalization of Fluorescent Probes: Accurate and Precise Registration with Nanometer Resolution. In Single-Molecule Techniques: A Laboratory Manual, P.R. Selvin and T. Ha, eds. (Woodbury, NY: Cold Spring Harbor Laboratory Press), pp. 73-84.

Cimini, D., Howell, B., Maddox, P., Khodjakov, A., Degrassi, F., and Salmon, E.D. (2001). Merotelic kinetochore orientation is a major mechanism of aneuploidy in mitotic mammalian tissue cells. J Cell Biol *153*, 517-527.

DeLuca, J.G., Dong, Y., Hergert, P., Strauss, J., Hickey, J.M., Salmon, E.D., and McEwen, B.F. (2005). Hec1 and nuf2 are core components of the kinetochore outer plate essential for organizing microtubule attachment sites. Mol Biol Cell *16*, 519-531.

DeLuca, J.G., Gall, W.E., Ciferri, C., Cimini, D., Musacchio, A., and Salmon, E.D. (2006). Kinetochore microtubule dynamics and attachment stability are regulated by Hec1. Cell *127*, 969-982.

Dong, Y., Vanden Beldt, K.J., Meng, X., Khodjakov, A., and McEwen, B.F. (2007). The outer plate in vertebrate kinetochores is a flexible network with multiple microtubule interactions. Nat Cell Biol *9*, 516-522.

Gerlich, D., Beaudouin, J., Kalbfuss, B., Daigle, N., Eils, R., and Ellenberg, J. (2003). Global chromosome positions are transmitted through mitosis in mammalian cells. Cell *112*, 751-764.

Howell, B.J., Hoffman, D.B., Fang, G., Murray, A.W., and Salmon, E.D. (2000). Visualization of Mad2 dynamics at kinetochores, along spindle fibers, and at spindle poles in living cells. J Cell Biol *150*, 1233-1250.

Hussein, D., and Taylor, S.S. (2002). Farnesylation of Cenp-F is required for G2/M progression and degradation after mitosis. J Cell Sci *115*, 3403-3414.

Kiyomitsu, T., Obuse, C., and Yanagida, M. (2007). Human Blinkin/AF15q14 is required for chromosome alignment and the mitotic checkpoint through direct interaction with Bub1 and BubR1. Dev Cell *13*, 663-676.

Kline, S.L., Cheeseman, I.M., Hori, T., Fukagawa, T., and Desai, A. (2006). The human Mis12 complex is required for kinetochore assembly and proper chromosome segregation. J Cell Biol *173*, 9-17.

Liao, H., Winkfein, R.J., Mack, G., Rattner, J.B., and Yen, T.J. (1995). CENP-F is a protein of the nuclear matrix that assembles onto kinetochores at late G2 and is rapidly degraded after mitosis. J Cell Biol *130*, 507-518.

Liu, S.T., Hittle, J.C., Jablonski, S.A., Campbell, M.S., Yoda, K., and Yen, T.J. (2003). Human CENP-I specifies localization of CENP-F, MAD1 and MAD2 to kinetochores and is essential for mitosis. Nat Cell Biol *5*:341–345.

Liu, S.T., Rattner, J.B., Jablonski, S.A., and Yen, T.J. (2006). Mapping the assembly pathways that specify formation of the trilaminar kinetochore plates in human cells. J Cell Biol *175*, 41-53.

McCleland, M.L., Kallio, M.J., Barrett-Wilt, G.A., Kestner, C.A., Shabanowitz, J., Hunt, D.F., Gorbsky, G.J., and Stukenberg, P.T. (2004). The vertebrate Ndc80 complex contains Spc24 and Spc25 homologs, which are required to establish and maintain kinetochore-microtubule attachment. Curr Biol *14*, 131-137.

Rieder, C.L. (1981). The structure of the cold-stable kinetochore fiber in metaphase PtK1 cells. Chromosoma *84*, 145-158.

Rusan, N.M., Fagerstrom, C.J., Yvon, A.M., and Wadsworth, P. (2001). Cell cycle-dependent changes in microtubule dynamics in living cells expressing green fluorescent protein-alpha tubulin. Mol Biol Cell *12*, 971-980.

Taylor, S.S., Hussein, D., Wang, Y., Elderkin, S., and Morrow, C.J. (2001). Kinetochore localisation and phosphorylation of the mitotic checkpoint components Bub1 and BubR1 are differentially regulated by spindle events in human cells. J Cell Sci *114*, 4385-4395.

Thomann, D., Rines, D.R., Sorger, P.K., and Danuser, G. (2002). Automatic fluorescent tag detection in 3D with super-resolution: application to the analysis of chromosome movement. J Microsc *208*, 49-64.

Yeh, E., Haase, J., Paliulis, L.V., Joglekar, A., Bond, L., Bouck, D., Salmon, E.D., and Bloom, K.S. (2008). Pericentric chromatin is organized into an intramolecular loop in mitosis. Curr Biol *18*, 81-90.

Zecevic, M., Catling, A.D., Eblen, S.T., Renzi, L., Hittle, J.C., Yen, T.J., Gorbsky, G.J., and Weber, M.J. (1998). Active MAP kinase in mitosis: localization at kinetochores and association with the motor protein CENP-E. J Cell Biol *142*, 1547-1558.